Chemical Science

ROYAL SOCIETY OF CHEMISTRY

EDGE ARTICLE

View Article Online
View Journal | View Issue

Cite this: *Chem. Sci.*, 2024, **15**, 8530

All publication charges for this article have been paid for by the Royal Society of Chemistry

A robust aluminum-octacarboxylate framework with scu topology for selective capture of sulfur dioxide†

Liang Yu,‡[ab] Meng He, ‡[c] Jinze Yao,‡[a] Qibin Xia, *[a] Sihai Yang,*[cd] Jing Li *[be] and Hao Wang *[b]

Received 19th March 2024
Accepted 30th April 2024

DOI: 10.1039/d4sc01877j

rsc.li/chemical-science

The high structural diversity and porosity of metal–organic frameworks (MOFs) promote their applications in selective gas adsorption. The development of robust MOFs that are stable against corrosive SO_2 remains a daunting challenge. Here, we report a highly robust aluminum-based MOF (HIAM-330) built on a 4-connected $Al_3(OH)_2(COO)_4$ cluster and 8-connected octacarboxylate ligand with a (4,8)-connected **scu** topology. It exhibits a fully reversible SO_2 uptake of 12.1 mmol g^{-1} at 298 K and 1 bar. It is capable of selective capture of SO_2 over other gases (CO_2, CH_4, and N_2) with high adsorption selectivities of 60, 330, and 3537 for equimolar mixtures of SO_2/CO_2, SO_2/CH_4, and SO_2/N_2, respectively, at 298 K and 1 bar. Breakthrough measurements verified the capability of HIAM-330 for selective capture of SO_2 (2500 ppm) over CO_2 or N_2. High-resolution synchrotron X-ray powder diffraction of SO_2 loaded HIAM-330 revealed the binding domains of adsorbed SO_2 molecules and host–guest interactions.

Introduction

By 2050, fossil fuels are predicted to account for 77% of global energy production, with coal emerging as the primary source in the global energy supply matrix.[1] Exhaust gases from pulverized coal combustion consist of 10–12% CO_2 and 500–3000 ppm SO_2;[2] the latter is a toxic and corrosive gas that will pose significant threats to human health and the environment.[3,4] While current flue gas desulfurization (FGD) technologies can remove most SO_2 from flue gases,[5–7] they generate a tremendous amount of solid waste and suffer from high energy input. Achieving complete removal of trace SO_2 proves challenging, as it necessitates a capture system with low selectivity for both dinitrogen and carbon dioxide coupled with remarkable material stability to withstand the highly corrosive nature of SO_2.[8,9]

Selective capture of SO_2 by dry, regenerable adsorbents under ambient conditions has attracted growing interest and is perceived as a promising strategy for eliminating trace SO_2.[10] This new method offers advantages such as lower energy consumption and minimized solid waste compared with the FGD strategy. Additionally, the recovered SO_2 can be used to produce valuable chemicals such as sulfuric acid. While porous materials such as zeolites,[8] activated carbon,[11] and silica[12] have been employed for SO_2 capture, their adsorption capacity is generally low,[13,14] limiting the overall capture efficiency. Metal–organic frameworks (MOFs) have garnered substantial attention for gas adsorption, due to their high porosity, structural diversity, precisely tunable pore dimensions, and highly customizable functionality.[9,15,16] However, to date, only a limited number of MOFs have exhibited reversible SO_2 adsorption and structural stability upon adsorption–desorption cycles.[17–19] This is due to the highly corrosive nature of SO_2, which can cause framework degradation in many MOFs.[1,20–22] Thus, the ability of a MOF to maintain its structural integrity and retain its adsorption capacity after repeated cycles of SO_2 adsorption and desorption is a crucial factor for its practical application in desulfurization processes. Furthermore, highly stable and crystalline MOFs can enable the study of host–guest interactions using *in situ* X-ray diffraction techniques to understand the underlying mechanism of selective adsorption. To this end, the development of MOFs with reversible SO_2 adsorption and excellent structural stability remains a challenging and important area of research.

Over the past few years, Al-MOFs and Zr-MOFs have demonstrated superior efficacy in the adsorption of SO_2,

[a]*School of Chemistry and Chemical Engineering, South China University of Technology, Guangzhou 510640, P. R. China. E-mail: qbxia@scut.edu.cn*

[b]*Hoffmann Institute of Advanced Materials, Shenzhen Polytechnic, 7098 Liuxian Blvd., Nanshan, Shenzhen 518055, P. R. China. E-mail: wanghao@szpt.edu.cn*

[c]*Department of Chemistry, University of Manchester, Manchester M13 9PL, UK*

[d]*Beijing National Laboratory for Molecular Sciences, College of Chemistry and Molecular Engineering, Peking University, Beijing 100871, China. E-mail: Sihai.Yang@pku.edu.cn*

[e]*Department of Chemistry and Chemical Biology, Rutgers University, 123 Bevier Road, Piscataway, NJ, 08854, USA. E-mail: jingli@rutgers.edu*

† Electronic supplementary information (ESI) available. CCDC 2303434 and 2258222. For ESI and crystallographic data in CIF or other electronic format see DOI: https://doi.org/10.1039/d4sc01877j

‡ These authors contributed equally.

underpinned by their high stability.[23,24] Their framework robustness arises not only from the strong Al–O and Zr–O bonds but also from the highly connected multinuclear inorganic clusters.[25] The ability of these clusters to link with multiple ligands bolsters the stability of the MOFs. Using highly connected organic ligands to synthesize MOFs is an effective strategy for improving framework stability. Thus, the combination of multinuclear inorganic building blocks and multitopic organic linkers usually leads to MOFs with intriguing connectivity and topology. However, the construction of MOFs from high valence metals (Al^{3+}, Zr^{4+}, Ti^{4+}, *etc.*) and organic linkers with high connectivity (>6) is particularly challenging due to the inherent synthetic difficulties. For example, only a handful of Zr-MOFs built on hexacarboxylates and octacarboxylates[26–30] have been reported, while only a single example of Al-MOF incorporating hexacarboxylates exists.[31] Yet, no examples of Al-MOFs made of an octacarboxylate linker have been reported to date.

Here, we report the incorporation of an octacarboxylate, 4′,4‴,4⁗,4⁗′-(ethene-1,1,2,2-tetrayl)tetrakis(([1,1′-biphenyl]-3,5-dicarboxylic acid)) (H_8ettbpdc) into a robust aluminum-based MOF, denoted as HIAM-330. It features a 4,8-c **scu** topology, built on 4-connected $Al_3O_2(COO)_4$ clusters and 8-connected ettbpdc^{8-} linkers. The structure contains two distinct types of cavities and demonstrates a SO_2 adsorption capacity of 12.1 mmol g^{-1} at 298 K and 1 bar. The adsorption was fully reversible and the adsorption capacity was retained after multiple SO_2 adsorption/desorption cycles. HIAM-330 exhibits selective capture of SO_2 in the presence of CO_2 and N_2. Molecular insights into the selective adsorption mechanism were achieved through X-ray diffraction analysis on SO_2-loaded HIAM-330, which elucidated the binding domains and host–guest interactions.

Results and discussion

H_8ettbpdc was selected as the organic building block for constructing the Al-octacarboxylate MOF due to its well-defined rigidity, planar geometry and facile synthesis. It was synthesized from 1,1,2,2-tetrakis(4-bromophenyl)ethylene *via* the Suzuki coupling reaction (Fig. S1–S3†). Subsequently, block-shaped crystals of HIAM-330 were solvothermally synthesized at 150 °C by reacting $Al(NO_3)_3 \cdot 9H_2O$ and H_8ettbpdc in DMF/formic acid/acetonitrile mixed solvent (Fig. S5†). Single-crystal X-ray diffraction analysis revealed that it crystallized in the tetragonal crystal system with a space group of *I*4/*mmm* (Table S1†). The crystal structure of HIAM-330 is built on a trinuclear $Al_3O_2(COO)_4(H_2O)_6$ cluster. In each cluster, the central Al^{3+} is octahedrally coordinated to four carboxylate oxygen atoms and two bridging oxygen atoms, while the terminal Al^{3+} is octahedrally connected to two carboxylate oxygen atoms, one bridging oxygen atom, and three water molecules (Fig. 1 and S6†). Thus, the trinuclear Al_3 clusters act as 4-connected nodes in the structure of HIAM-330, bridged by ettbpdc^{8-} organic struts. It is noteworthy that the Al_3 cluster observed here is distinct from the commonly observed triangular trinuclear Al_3 SBU, where a μ_3-O connects three Al^{3+} to form a 6-connected node.[25] The octacarboxylate organic linker ettbpdc^{8-} is fully deprotonated and connected to sixteen Al^{3+} centers from eight Al_3 clusters, with all carboxylates coordinated in bidentate mode (Fig. S7†). The overall structure of HIAM-330 features 4,8-c **scu** topology. It is intriguing that its connectivity is in sharp contrast to that of previously reported **scu** Zr-MOFs. The latter, as exemplified in PCN-606,[32] is constructed on 8-connected Zr_6 nodes and 4-connected organic linkers (usually tetracarboxylates, Fig. 1). Nevertheless, in HIAM-330, the Al_3 clusters serve as the 4-connected nodes and the organic ligands act as the 8-connected

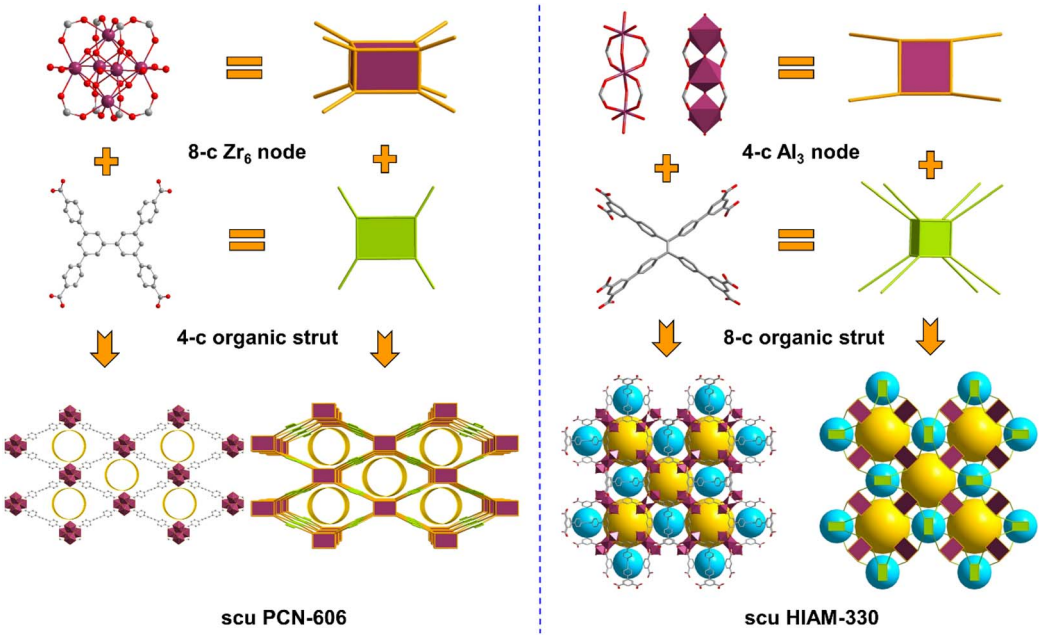

Fig. 1 Building blocks and crystal structure of PCN-660 (left) and HIAM-330 (right).

units. This also leads to a different pore structure. The commonly observed **scu**-type Zr-MOFs such as PCN-606 or Zr-abtc possess one-dimensional rhombic channels, derived from the cubic cages of 4,12-c **ftw**-type connectivity.[33] In contrast, in HIAM-330, there are two distinct types of cages, with large and small cages arrayed in alternating sequences (Fig. 1 and S8†).

The phase purity of HIAM-330 was verified through powder X-ray diffraction (PXRD) analysis (Fig. 2a). Thermogravimetric analysis (TGA) of as-synthesized HIAM-330 displayed a continuous weight loss, while that of the methanol-exchanged sample showed a plateau from 120–270 °C, indicating the successful exchange of high boiling point solvents by methanol (Fig. S9†). During the subsequent activation of the methanol-exchanged HIAM-330 by heating at 150 °C, its crystal structure was fully retained. Our experimental investigation suggests that HIAM-330 exhibits excellent stability, as evidenced by its fully preserved PXRD patterns after being heated at 150 °C in open air for 1 week, immersed in water at 80 °C for 1 week, or exposed to 90% humidity for 1 week (Fig. 2a). The permanent porosity of HIAM-330 was evaluated by N_2 adsorption measurements at 77 K (Fig. 2b). The N_2 isotherm displays a typical type I profile, yielding a BET surface area of 1624 $m^2\ g^{-1}$ and a pore volume of 0.65 $m^3\ g^{-1}$ (Fig. S10†). The pore size distribution curve, determined using the NLDFT model, was centered at approximately 5.5, 8.5, and 13.0 Å (Fig. S11†), which is consistent with the value estimated from Zeo++ software based on the crystal structure (Fig. S12†).

Single-component adsorption isotherms of SO_2 were collected at 298, 283, and 273 K (Fig. S13†). HIAM-330 exhibits fully reversible adsorption for SO_2 with a high adsorption uptake of 12.1 mmol g^{-1} at 298 K and 1 bar. This value is higher than those of most of the MOFs studied for SO_2 capture, such as Zr-bptc, UiO-66, UiO-66–NH_2, and Zr-DMTDC,[24] but is lower than those of the recently reported MFM-190 series showing higher porosity[34] (Fig. S14†). Furthermore, the adsorption uptake increased dramatically at relatively low pressure, indicating its ability to capture trace SO_2. The calculated isosteric heat of adsorption (Q_{st}) is 38.0 kJ mol^{-1} at zero coverage. To study the capability of HIAM-330 for selective capture of SO_2 from other light gases that often co-exist in the flue-gas stream, its adsorption towards CO_2, CH_4, and N_2 was also evaluated. HIAM-330 adsorbs 2.60 mmol g^{-1} of CO_2, 0.68 mmol g^{-1} of CH_4, and 0.09 mmol g^{-1} of N_2 at 1 bar and 298 K, substantially lower than that of SO_2 (Fig. 2c). The Q_{st} of CO_2 calculated from adsorption isotherms at 298, 283, and 273 K is 16 kJ mol^{-1} at zero coverage, indicating its notably weaker adsorption affinity compared to that of SO_2 (Fig. 2e). The selectivities of HIAM-330 for SO_2/CO_2, SO_2/N_2 and SO_2/CH_4 were calculated *via* ideal adsorbed solution theory (IAST) at 298 K (Fig. 2d). Due to the negligible adsorption capacity for nitrogen, the calculated SO_2/N_2 selectivity values are unusually high (>1000) and are subject to large uncertainties. HIAM-330 also shows high selectivity values of 60 and 330 for equimolar binary mixtures of SO_2/CO_2 and SO_2/CH_4, respectively at 298 K and a total pressure of 1 bar. The values remain similar when the concentration of SO_2 decreased to 10%, resulting in selectivities of 44 and 239 for SO_2/CO_2 and SO_2/CH_4, respectively. These results suggest the preferential adsorption of SO_2 over other light gases by HIAM-330.

While many MOF materials exhibit high adsorption capacities for SO_2 due to high porosity, only a small number of them show fully reversible adsorption and retain their crystallinity when exposed to highly corrosive SO_2. HIAM-330 demonstrates the ability to maintain its structure after undergoing SO_2 adsorption–desorption tests (Fig. 2a). In consideration of practical applications, cyclic adsorption–desorption experiments were also conducted. In five consecutive adsorption/

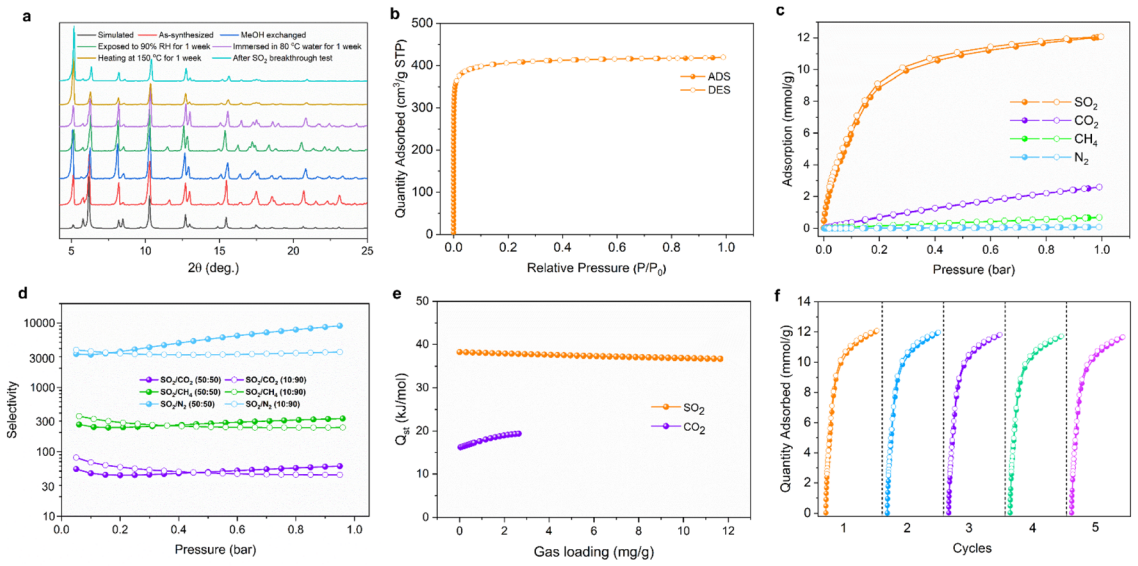

Fig. 2 Gas adsorption on HIAM-330. (a) PXRD patterns of HIAM-330 under various conditions. (b) Adsorption–desorption isotherms of N_2 at 77 K by HIAM-330. (c) Adsorption isotherms of SO_2, CO_2, CH_4, and N_2 at 298 K. (d) IAST selectivities of SO_2/CO_2, SO_2/CH_4, and SO_2/N_2 at 298 K in HIAM-330. (e) Q_{st} curves for SO_2 and CO_2 in HIAM-330. (f) Five adsorption–desorption cycles for SO_2 in HIAM-330 at 298 K and 1 bar.

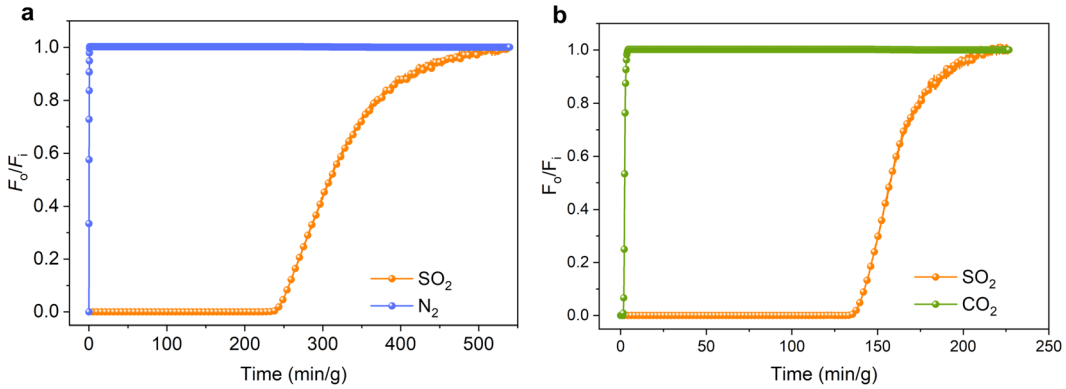

Fig. 3 Separation of SO_2, N_2 and CO_2 by HIAM-330: breakthrough plots for (a) the SO_2/N_2 mixture (2500 ppm SO_2, 75% N_2 in He, and total flow rate: 20 mL min^{-1}) and (b) the SO_2/CO_2 mixture (2500 ppm SO_2, 15% CO_2 in He, and total flow rate: 20 mL min^{-1}) in HIAM-330 at 298 K.

desorption cycles, no notable loss of SO_2 adsorption capacity (<5%) was observed for HIAM-330 (Fig. 2f), further confirming its high stability to SO_2.

To further verify the ability of HIAM-330 for selective capture of trace SO_2, dynamic breakthrough experiments were conducted using a fixed bed filled with HIAM-330. At 298 K and 1 bar, a mixture of SO_2/N_2 (2500 ppm SO_2, 75% N_2 diluted in He) was passed through the column at a flow rate of 20 mL min^{-1}. The results showed that N_2 eluted at the beginning of the process, while SO_2 was retained in the column for more than three hours (Fig. 3a). Additionally, the calculated SO_2/N_2 separation factor was 745. Similarly, another column breakthrough measurement was performed with a mixture of SO_2/CO_2 (2500 ppm SO_2, 15% CO_2 diluted in He). CO_2 broke through within less than two minutes, while SO_2 was retained for 136 minutes (Fig. 3b). The separation factor of SO_2/CO_2 was calculated to be 65.5. These findings validated the capability of HIAM-330 for selective capture of trace SO_2 from other light gases as a durable adsorbent.

The adsorption domains of SO_2 in HIAM-330 were determined by Rietveld refinements of the high-resolution synchrotron PXRD pattern of SO_2-loaded HIAM-330 (Fig. S22†). The robust framework of HIAM-330 remained highly crystalline, allowing direct visualization of the adsorbed SO_2 molecules in the pores. It was revealed that there were seven SO_2 binding sites in the pores, with one in the small tetrahedral cage (Fig. 4a), two in the large octahedral cage (Fig. 4b), and four in the small pocket surrounded by eight trinuclear Al_3 clusters (Fig. 4c). The total crystallographic uptake of SO_2 was estimated to be 7.35 mmol g^{-1}, corresponding to a crystal structure at a relatively low SO_2 pressure of ~0.14 bar. It is interesting to observe that most of the adsorbed SO_2 molecules are located

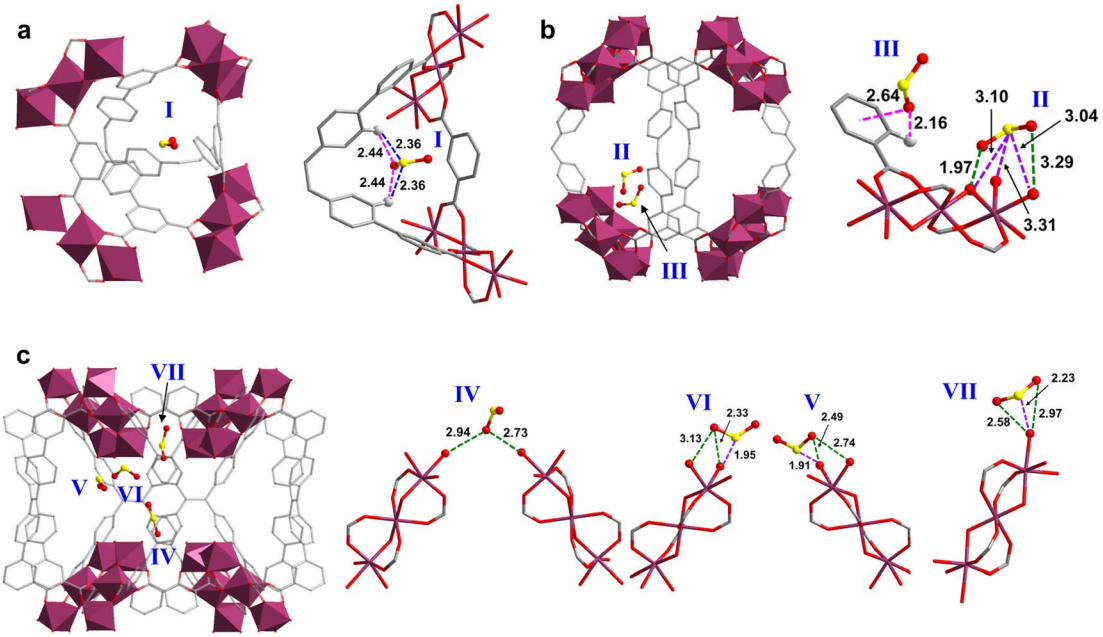

Fig. 4 Adsorption domains of SO_2 in HIAM-330 determined by Rietveld refinements of high-resolution *in situ* synchrotron powder X-ray diffraction. (a) site I, (b) sites II and III, (c) sites IV–VII.

nearby the inorganic nodes rather than aggregating in the two main cages. This indicates that the Al_3 clusters are favorable binding sites for SO_2 at low pressure. The SO_2 molecule at site I was stabilized by the organic linker through hydrogen bonds (OSO···H–C = 2.44 Å and O_2S···H–C = 2.36 Å). At site III, the adsorbed SO_2 was immobilized by the phenyl ring (OSO···pi = 2.64 Å, electrostatic interactions) and by one hydrogen bond (OSO···H–C = 2.16 Å). In the remaining five sites (sites II and IV–VII), the adsorbed SO_2 molecules were predominantly interacting with the Al_3 cluster (the bridging oxygen or the terminal H_2O) through dipole–dipole interactions with the shortest OSO···O and O_2S···O distances of 1.97 and 1.91 Å, respectively. The above results offer molecular insights into the guest–host interaction of SO_2 adsorption in HIAM-330 and highlight the important role of the trinuclear Al_3 cluster in SO_2 capture.

Conclusions

The design and synthesis of highly porous and stable MOFs with multi-topic ligands and high valence metals is important for enriching MOF structure diversity, adsorption, and capture of corrosive gases such as SO_2. We present the construction of an intriguing 4,8-c **scu**-type Al-MOF using a rigid octacarboxylate linker. The resulting MOF, HIAM-330, exhibits high porosity, excellent stability, high SO_2 uptake (12.08 mmol g^{-1} at 298 K and 1 bar), and high IAST SO_2/CO_2 selectivity (60, SO_2/CO_2 = 50/50). Mixed-gas column breakthrough experiments further confirmed the effective removal of trace SO_2 by HIAM-330 in the presence of CO_2 and N_2. The excellent chemical and thermal stability of HIAM-330 endows it with good recyclability. Further, Rietveld refinement of high-resolution PXRD patterns of SO_2-loaded HIAM-330 provides valuable information regarding SO_2 adsorption sites and possible guest–host interactions, which is important for understanding the adsorption mechanism. Overall, our findings contribute to rational design strategies for making stable MOFs that hold strong promise for effective capture of target molecules.

Data availability

Data associated to the article are available in the ESI.†

Author contributions

Liang Yu: investigation, methodology, and writing – original draft. Meng He: investigation and methodology. Jinze Yao: investigation and validation. Qibin Xia: conceptualization, supervision, project administration, and writing – review & editing. Sihai Yang: conceptualization, project administration, supervision, and writing – review & editing. Jing Li: conceptualization, supervision, project administration, and writing – review & editing. Hao Wang: conceptualization, supervision, and writing – review & editing.

Conflicts of interest

The authors declare that they have no competing interests.

Acknowledgements

This work was supported financially by the Shenzhen Science and Technology Program (No. KCXFZ20211020163818026) and National Natural Science Foundation of China (22178119). Work in the US was supported by the U.S. Department of Energy, Office of Science, Office of Basic Energy Sciences under Award No. DE-SC0019902.

Notes and references

1 J. H. Carter, X. Han, F. Y. Moreau, I. da Silva, A. Nevin, H. G. W. Godfrey, C. C. Tang, S. Yang and M. Schröder, Exceptional Adsorption and Binding of Sulfur Dioxide in a Robust Zirconium-Based Metal-Organic Framework, *J. Am. Chem. Soc.*, 2018, **140**, 15564–15567.

2 M. Savage, Y. Cheng, T. L. Easun, J. E. Eyley, S. P. Argent, M. R. Warren, W. Lewis, C. Murray, C. C. Tang, M. D. Frogley, G. Cinque, J. Sun, S. Rudić, R. T. Murden, M. J. Benham, A. N. Fitch, A. J. Blake, A. J. Ramirez-Cuesta, S. Yang and M. Schröder, Selective Adsorption of Sulfur Dioxide in a Robust Metal-Organic Framework Material, *Adv. Mater.*, 2016, **28**, 8705–8711.

3 M. Kampa and E. Castanas, Human health effects of air pollution, *Environ. Pollut.*, 2008, **151**, 362–367.

4 N. Greenberg, R. Carel and B. A. Portnov, Air Pollution and Respiratory Morbidity in Israel: A Review of Accumulated Empiric Evidence, *Isr. Med. Assoc. J.*, 2015, **17**, 445–450.

5 G. T. Rochelle, Amine scrubbing for CO2 capture, *Science*, 2009, **325**, 1652–1654.

6 G. Cui, J. Wang and S. Zhang, Active chemisorption sites in functionalized ionic liquids for carbon capture, *Chem. Soc. Rev.*, 2016, **45**, 4307–4339.

7 R. K. Srivastava and W. Jozewicz, Flue gas desulfurization: the state of the art, *J. Air Waste Manag. Assoc.*, 2001, **51**, 1676–1688.

8 I. Matito-Martos, A. Martin-Calvo, J. J. Gutiérrez-Sevillano, M. Haranczyk, M. Doblare, J. B. Parra, C. O. Ania and S. Calero, Zeolite screening for the separation of gas mixtures containing SO2, CO2 and CO, *Phys. Chem. Chem. Phys.*, 2014, **16**, 19884–19893.

9 D. M. D'Alessandro, B. Smit and J. R. Long, Carbon dioxide capture: prospects for new materials, *Angew. Chem., Int. Ed.*, 2010, **49**, 6058–6082.

10 G. L. Smith, J. E. Eyley, X. Han, X. Zhang, J. Li, N. M. Jacques, H. G. W. Godfrey, S. P. Argent, L. J. M. McPherson, S. J. Teat, Y. Cheng, M. D. Frogley, G. Cinque, S. J. Day, C. C. Tang, T. L. Easun, S. Rudić, A. J. Ramirez-Cuesta, S. Yang and M. Schröder, Reversible coordinative binding and separation of sulfur dioxide in a robust metal-organic framework with open copper sites, *Nat. Mater.*, 2019, **18**, 1358–1365.

11 X. Zhou, H. Yi, X. Tang, H. Deng and H. Liu, Thermodynamics for the adsorption of SO2, NO and CO2 from flue gas on activated carbon fiber, *Chem. Eng. J.*, 2012, **200–202**, 399–404.
12 Z. Zhang, L. Wu, J. Dong, B.-G. Li and S. Zhu, Preparation and SO2 Sorption/Desorption Behavior of an Ionic Liquid Supported on Porous Silica Particles, *Ind. Eng. Chem. Res.*, 2009, **48**, 2142–2148.
13 E. Raymundo-Piñero, D. Cazorla-Amorós, C. Salinas-Martinez de Lecea and A. Linares-Solano, Factors controling the SO2 removal by porous carbons: relevance of the SO2 oxidation step, *Carbon*, 2000, **38**, 335–344.
14 Y. Mathieu, L. Tzanis, M. Soulard, J. Patarin, M. Vierling and M. Molière, Adsorption of SOx by oxide materials: a review, *Fuel Process. Technol.*, 2013, **114**, 81–100.
15 X. Lin, N. R. Champness and M. Schröder, Hydrogen, methane and carbon dioxide adsorption in metal-organic framework materials, *Top. Curr. Chem.*, 2010, **293**, 35–76.
16 Q. Li, W. Zhang, O. S. Miljanić, C. H. Sue, Y. L. Zhao, L. Liu, C. B. Knobler, J. F. Stoddart and O. M. Yaghi, Docking in metal-organic frameworks, *Science*, 2009, **325**, 855–859.
17 T. G. Glover, G. W. Peterson, B. J. Schindler, D. Britt and O. Yaghi, MOF-74 building unit has a direct impact on toxic gas adsorption, *Chem. Eng. Sci.*, 2011, **66**, 163–170.
18 K. Tan, N. Nijem, P. Canepa, Q. Gong, J. Li, T. Thonhauser and Y. J. Chabal, Stability and Hydrolyzation of Metal Organic Frameworks with Paddle-Wheel SBUs upon Hydration, *Chem. Mater.*, 2012, **24**, 3153–3167.
19 G. L. Smith, J. E. Eyley, X. Han, X. Zhang, J. Li, N. M. Jacques, H. G. W. Godfrey, S. P. Argent, L. J. M. McPherson, S. J. Teat, Y. Cheng, M. D. Frogley, G. Cinque, S. J. Day, C. C. Tang, T. L. Easun, S. Rudić, A. J. Ramirez-Cuesta, S. Yang and M. Schröder, Reversible coordinative binding and separation of sulfur dioxide in a robust metal–organic framework with open copper sites, *Nat. Mater.*, 2019, **18**, 1358–1365.
20 S. Yang, J. Sun, A. J. Ramirez-Cuesta, S. K. Callear, W. I. David, D. P. Anderson, R. Newby, A. J. Blake, J. E. Parker, C. C. Tang and M. Schröder, Selectivity and direct visualization of carbon dioxide and sulfur dioxide in a decorated porous host, *Nat. Chem.*, 2012, **4**, 887–894.
21 S. M. Cohen, Postsynthetic Methods for the Functionalization of Metal–Organic Frameworks, *Chem. Rev.*, 2012, **112**, 970–1000.
22 T. Islamoglu, S. Goswami, Z. Li, A. J. Howarth, O. K. Farha and J. T. Hupp, Postsynthetic Tuning of Metal–Organic Frameworks for Targeted Applications, *Acc. Chem. Res.*, 2017, **50**, 805–813.
23 L. Li, I. da Silva, D. I. Kolokolov, X. Han, J. Li, G. Smith, Y. Cheng, L. L. Daemen, C. G. Morris, H. G. W. Godfrey, N. M. Jacques, X. Zhang, P. Manuel, M. D. Frogley, C. A. Murray, A. J. Ramirez-Cuesta, G. Cinque, C. C. Tang, A. G. Stepanov, S. Yang and M. Schroder, Post-synthetic modulation of the charge distribution in a metal-organic framework for optimal binding of carbon dioxide and sulfur dioxide, *Chem. Sci.*, 2019, **10**, 1472–1482.
24 J. Li, G. L. Smith, Y. Chen, Y. Ma, M. Kippax-Jones, M. Fan, W. Lu, M. D. Frogley, G. Cinque, S. J. Day, S. P. Thompson, Y. Cheng, L. L. Daemen, A. J. Ramirez-Cuesta, M. Schröder and S. Yang, Structural and Dynamic Analysis of Sulphur Dioxide Adsorption in a Series of Zirconium-Based Metal-Organic Frameworks, *Angew. Chem., Int. Ed.*, 2022, **61**, e202207259.
25 W. Fan, K.-Y. Wang, C. Welton, L. Feng, X. Wang, X. Liu, Y. Li, Z. Kang, H.-C. Zhou, R. Wang and D. Sun, Aluminum metal–organic frameworks: from structures to applications, *Coord. Chem. Rev.*, 2023, **489**, 215175.
26 W. Liu, E. Wu, B. Yu, Z. Liu, K. Wang, D. Qi, B. Li and J. Jiang, Reticular Synthesis of Metal-Organic Frameworks by 8-Connected Quadrangular Prism Ligands for Water Harvesting, *Angew. Chem., Int. Ed.*, 2023, **62**, e202305144.
27 B. Ortín-Rubio, C. Perona-Bermejo, J. A. S. D. Pino, F. J. Carmona, F. Gándara, J. A. R. Navarro, J. Juanhuix, I. Imaz and D. Maspoch, A mesoporous Zr-based metal-organic framework driven by the assembly of an octatopic linker, *Chem. Commun.*, 2023, **59**, 7803–7806.
28 P. T. K. Nguyen, H. T. D. Nguyen, H. N. Nguyen, C. A. Trickett, Q. T. Ton, E. Gutiérrez-Puebla, M. A. Monge, K. E. Cordova and F. Gándara, New Metal-Organic Frameworks for Chemical Fixation of CO(2), *ACS Appl. Mater. Interfaces*, 2018, **10**, 733–744.
29 Z. Chen, P. Li, X. Wang, K.-i. Otake, X. Zhang, L. Robison, A. Atilgan, T. Islamoglu, M. G. Hall, G. W. Peterson, J. F. Stoddart and O. K. Farha, Ligand-Directed Reticular Synthesis of Catalytically Active Missing Zirconium-Based Metal–Organic Frameworks, *J. Am. Chem. Soc.*, 2019, **141**, 12229–12235.
30 D. Alezi, I. Spanopoulos, C. Tsangarakis, A. Shkurenko, K. Adil, Y. Belmabkhout, M. O. Keeffe, M. Eddaoudi and P. N. Trikalitis, Reticular Chemistry at Its Best: Directed Assembly of Hexagonal Building Units into the Awaited Metal-Organic Framework with the Intricate Polybenzene Topology, pbz-MOF, *J. Am. Chem. Soc.*, 2016, **138**, 12767–12770.
31 Z. Chen, P. Li, R. Anderson, X. Wang, X. Zhang, L. Robison, L. R. Redfern, S. Moribe, T. Islamoglu, D. A. Gómez-Gualdrón, T. Yildirim, J. F. Stoddart and O. K. Farha, Balancing volumetric and gravimetric uptake in highly porous materials for clean energy, *Science*, 2020, **368**, 297–303.
32 J. Pang, S. Yuan, J. Qin, C. Liu, C. Lollar, M. Wu, D. Yuan, H. C. Zhou and M. Hong, Control the Structure of Zr-Tetracarboxylate Frameworks through Steric Tuning, *J. Am. Chem. Soc.*, 2017, **139**, 16939–16945.
33 H. Wang, X. Dong, J. Lin, S. J. Teat, S. Jensen, J. Cure, E. V. Alexandrov, Q. Xia, K. Tan, Q. Wang, D. H. Olson, D. M. Proserpio, Y. J. Chabal, T. Thonhauser, J. Sun, Y. Han and J. Li, Topologically guided tuning of Zr-MOF pore structures for highly selective separation of C6 alkane isomers, *Nat. Commun.*, 2018, **9**, 1745.
34 W. Li, J. Li, T. D. Duong, S. A. Sapchenko, X. Han, J. D. Humby, G. F. S. Whitehead, I. J. Victórica-Yrezábal, I. da Silva, P. Manuel, M. D. Frogley, G. Cinque, M. Schröder and S. Yang, Adsorption of Sulfur Dioxide in Cu(II)-Carboxylate Framework Materials: The Role of Ligand Functionalization and Open Metal Sites, *J. Am. Chem. Soc.*, 2022, **144**, 13196–13204.